

Structural Similarities and Differences between Two Functionally Distinct SecA Proteins, *Mycobacterium tuberculosis* SecA1 and SecA2

Stephanie Swanson,^a Thomas R. Ioerger,^b Nathan W. Rigel,^{c*} Brittany K. Miller,^c Miriam Braunstein,^c James C. Sacchettini^a

Department of Biochemistry & Biophysics^a and Department of Computer Science and Engineering,^b Texas A&M University, College Station, Texas, USA; Department of Microbiology and Immunology, University of North Carolina—Chapel Hill, Chapel Hill, North Carolina, USA^c

ABSTRACT

While SecA is the ATPase component of the major bacterial secretory (Sec) system, mycobacteria and some Gram-positive pathogens have a second paralog, SecA2. In bacteria with two SecA paralogs, each SecA is functionally distinct, and they cannot compensate for one another. Compared to SecA1, SecA2 exports a distinct and smaller set of substrates, some of which have roles in virulence. In the mycobacterial system, some SecA2-dependent substrates lack a signal peptide, while others contain a signal peptide but possess features in the mature protein that necessitate a role for SecA2 in their export. It is unclear how SecA2 functions in protein export, and one open question is whether SecA2 works with the canonical SecYEG channel to export proteins. In this study, we report the structure of *Mycobacterium tuberculosis* SecA2 (*MtbSecA2*), which is the first structure of any SecA2 protein. A high level of structural similarity is observed between SecA2 and SecA1. The major structural difference is the absence of the helical wing domain, which is likely to play a role in how *MtbSecA2* recognizes its unique substrates. Importantly, structural features critical to the interaction between SecA1 and SecYEG are preserved in SecA2. Furthermore, suppressor mutations of a dominant-negative *secA2* mutant map to the surface of SecA2 and help identify functional regions of SecA2 that may promote interactions with SecYEG or the translocating polypeptide substrate. These results support a model in which the mycobacterial SecA2 works with SecYEG.

IMPORTANCE

SecA2 is a paralog of SecA1, which is the ATPase of the canonical bacterial Sec secretion system. SecA2 has a nonredundant function with SecA1, and SecA2 exports a distinct and smaller set of substrates than SecA1. This work reports the crystal structure of SecA2 of *Mycobacterium tuberculosis* (the first SecA2 structure reported for any organism). Many of the structural features of SecA1 are conserved in the SecA2 structure, including putative contacts with the SecYEG channel. Several structural differences are also identified that could relate to the unique function and selectivity of SecA2. Suppressor mutations of a *secA2* mutant map to the surface of SecA2 and help identify functional regions of SecA2 that may promote interactions with SecYEG.

SecA is the ATPase component of the bacterial Sec secretion pathway (1). SecA recognizes proteins destined for export from the cytoplasm and provides energy to translocate them across the cytoplasmic membrane by way of the SecYEG translocase channel. The proteins exported by SecA are synthesized as preproteins with N-terminal signal peptides. Following translocation, the signal peptide is cleaved to release the mature protein species. Both the signal peptide and features of the mature protein are recognized by SecA (2). Some Gram-positive and acid-fast bacteria, including mycobacteria, have a SecA paralog referred to as SecA2. SecA1, the canonical SecA in these organisms, is essential for growth and responsible for the majority of protein export that occurs. In contrast, SecA2 is typically not essential and is required for the export of a more limited subset of proteins (3, 4). Studies in mycobacteria show that even when overexpressed, the two SecA proteins are unable to compensate for each other (5). Thus, each SecA protein has distinct functions in protein export. In *Mycobacterium tuberculosis*, SecA2 (*MtbSecA2*) is not essential for growth in culture, but it is essential for virulence *in vivo* (6, 7). Furthermore, SecA2 is required for intracellular growth of *M. tuberculosis* in macrophages (8). The role of SecA2 in promoting growth in macrophages is attributed to a role in preventing phagosome maturation (9). In *Mycobacterium marinum*, export of protein kinase G (PknG) by the SecA2 pathway is suggested to at least be partially responsible for the SecA2 effect on phagosome matu-

ration (10). In *M. tuberculosis*, the SecA2 pathway is additionally required to restrict apoptosis of infected macrophages. A possible explanation for the latter effect is the SecA2-dependent secretion of superoxide dismutase, which may reduce reactive oxygen species (ROS)-mediated apoptosis (11, 12). An association between SecA2 and the secretion of virulence factors extends to other bacterial pathogens as well (13–16). There is also an intriguing association between the SecA2 pathway and the export of S-layer proteins by some Gram-positive bacteria, such as *Bacillus anthracis* (17) and *Clostridium difficile* (18).

Received 29 August 2015 Accepted 1 December 2015

Accepted manuscript posted online 14 December 2015

Citation Swanson S, Ioerger TR, Rigel NW, Miller BK, Braunstein M, Sacchettini JC. 2016. Structural similarities and differences between two functionally distinct SecA proteins, *Mycobacterium tuberculosis* SecA1 and SecA2. *J Bacteriol* 198:720–730. doi:10.1128/JB.00696-15.

Editor: O. Schneewind

Address correspondence to James C. Sacchettini, sacchett@tamu.edu.

* Present address: Nathan W. Rigel, Department of Biology, Hofstra University, Hempstead, New York, USA.

Supplemental material for this article may be found at <http://dx.doi.org/10.1128/JB.00696-15>.

Copyright © 2016, American Society for Microbiology. All Rights Reserved.

It is unclear how *MtbSecA2* carries out its unique function in protein export. In some organisms with two SecAs, there is a SecY paralog (SecY2), with which SecA2 likely interacts (19). In SecA2-SecY2 systems, SecY2 and several accessory Sec proteins (Asp) are thought to form an accessory protein translocation channel in the cytoplasmic membrane (4). Mycobacteria, however, are in a group of bacteria referred to as “SecA2-only” systems that lack a second SecY ortholog (3). Mycobacteria, as well as several Gram-positive species, including *Listeria monocytogenes* (13), *Corynebacterium glutamicum* (20), and *C. difficile* (18), are in the “SecA2-only” group. An important but unresolved question is whether SecA2 works with the canonical SecYEG channel to export proteins in these systems lacking a second SecY.

The mycobacterial proteins currently known to be exported by SecA2 include examples with typical Sec signal peptides, as well as proteins lacking signal peptides altogether (3). Superoxide dismutase (SodA) in *M. tuberculosis* and PknG in *M. tuberculosis* and *M. marinum* are examples of proteins lacking signal peptides that are exported in a SecA2-dependent manner (7, 10, 21). Of the signal peptide-containing proteins exported by the SecA2 systems of *Mycobacterium smegmatis* (22), *M. marinum* (10), and *M. tuberculosis* (21), the most thoroughly studied proteins are the *M. smegmatis* 1704 (Ms1704) and Ms1712 proteins (22). Studies of Ms1704 and Ms1712 demonstrate that they require their signal peptide for export, but it is a feature of the mature portions of these proteins that necessitates export via the SecA2-dependent pathway (23). Interestingly, when fused to a signal peptide for the twin-arginine translocation (Tat) pathway, the mature domain of Ms1704 is exported by the Tat pathway. This result suggests that the defining feature of SecA2 substrates may be a tendency to fold prior to export (23). This is because proteins that get translocated across the membrane by the Tat pathway must be folded in the cytoplasm prior to export (24). In contrast, preproteins exported by the canonical SecA must be unfolded (25), sometimes with the help of export chaperones (26, 27), due to the narrow diameter of the SecYEG central channel. Therefore, if SecA2 works with SecYEG, the role of SecA2 may be to facilitate the export of proteins that have a tendency to fold prior to export by either helping to maintain such proteins in an unfolded state or assisting in the recognition or export of such problematic substrates.

There is only 38% amino acid sequence identity between the *MtbSecA1* and *MtbSecA2* proteins. Yet, SecA2, like SecA1, has a DEAD box ATPase domain (28), and ATPase activity is required for SecA2 function (29). Furthermore, SecA2 variants lacking ATPase activity due to an amino acid substitution in the Walker box are dominant negative, and a *secA2* dominant-negative mutant exhibits *secA2* mutant phenotypes (a growth defect on rich agar and azide sensitivity) that are more severe than those exhibited by a $\Delta secA2$ null mutant (29). Extragenic suppressors of this dominant-negative *secA2* allele map to the *secY* promoter, and increased SecY levels suppress the *secA2* dominant-negative phenotype (30). These findings suggest that the SecA2 dominant-negative protein is locked in a nonproductive interaction with the essential SecYEG channel, which inhibits SecYEG function but can be overcome by increased SecY production. This is consistent with SecA2 working with SecYEG. In a recent study of the SecA2-only system of *L. monocytogenes*, suppressors of a *secA2* mutation also mapped to *secY* (74). Furthermore, the behavior of a dominant-negative SecA1 mutant in the *C. difficile* system is consistent with the SecYEG translocase used by SecA1 also being used by

SecA2 (18). Thus, it seems likely that in these SecA2-only systems, SecY is involved. However, a direct interaction between SecA2 and SecYEG has not been demonstrated in any system.

Previously, the crystal structure of the canonical SecA1 was solved in *M. tuberculosis* (31), as well as several other organisms, including *Escherichia coli* (32), *Bacillus subtilis* (33), *Thermotoga maritima* (34), and *Thermus thermophilus* (35). SecA structures contain five canonical domains, organized roughly in the shape of a barbell: a core helical scaffold domain (HSD), forming the “axis”; 2 nucleotide-binding domains (NBD1 and NBD2), which together form a DEAD box, RecA-like, or superfamily II helicase motor domain on one end of the barbell; and a helical-wing domain (HWD) and preprotein cross-linking domain (PPXD) on the other end of the barbell. In addition, a helix-loop-helix domain called IRA1 (for “intramolecular regulator of ATPase”) packs against the HSD, with helices aligned in parallel. The loop connecting the helices of IRA1 is known as the two-helix finger (2HF). The 2HF has been shown to insert into the SecYEG pore, and it is proposed to promote forward movement of the preprotein through the channel (34, 36), although the interaction between the 2HF and SecYEG could also serve an alternate role besides pushing the translocating protein through the channel (37). During preprotein translocation, SecA undergoes significant conformational changes, one of which involves the orientation of the PPXD domain. According to one model (38), the PPXD likely starts out oriented toward the HWD, forming a hydrophobic “cleft” for binding the signal peptide of the preprotein (39, 40), and then rotates toward NBD2 to form a “clamp” around the translocating polypeptide chain, which has been proposed to be initiated by docking with SecYEG (41).

In order to better understand the unique function of SecA2, we solved the crystal structure of *MtbSecA2*, which is the first SecA2 structure to be determined in any organism. The structure reveals that the HWD domain is completely absent in *MtbSecA2*. The HWD could play a role in interacting with protein substrates, as it forms part of a cleft with the PPXD that is implicated in peptide binding (40). Although the residues that directly bind the signal peptide (based on nuclear magnetic resonance [NMR] studies) are contributed by the PPXD and IRA1 domains (40), the HWD would likely be physically proximal to the untranslocated portion of protein substrates. Furthermore, residues in the HWD of *E. coli* SecA (along with the PPXD and HSD) have been shown to cross-link with synthetic signal peptides in cysteine substitution experiments (42). The lack of an HWD in SecA2 leads to a signal peptide binding cleft that is more highly solvent exposed than in SecA1, which we propose could account for recognition of specific SecA2-dependent substrates and prevent export of the larger number of SecA1-dependent preproteins. The structure also reveals conservation in *MtbSecA2* of features critical to the interaction between SecA and SecYEG proteins. Finally, by mapping intragenic suppressor mutations onto the SecA2 structure, we show that the mutated residues appear in surface-exposed regions and map to three functional domains that are likely involved in mediating interactions with other protein partners, such as SecYEG.

MATERIALS AND METHODS

Protein expression and purification. The 778-residue open reading frame (ORF) of *MtbSecA2* was cloned into expression vector pNR14. Several genomic databases list *MtbSecA2* as having a total length of 808

amino acids (aa) (e.g., NCBI accession no. [NP_216337](#)). However, the start site in this annotation is likely to be incorrect, as the first 30 aa are not required for function and represent an N-terminal extension that is not observed in other SecA orthologs (28, 43). Therefore, we designate the GTG codon corresponding to residue 31 in the NCBI annotation as the true start codon, yielding a total ORF length of 778 aa. The expression construct pNR14 produces a tag-less form of the protein (28). Selenomethionyl protein was produced by transforming the *E. coli* methionine auxotroph B834(DE3) (Novagen) with the pNR14 expression vector. A 6-liter culture was grown under standard conditions to mid-log phase. The cells were pelleted and used to inoculate 12 liters of M9 minimal medium supplemented with 50 mg/liter of L-selenomethionine (SeMet), 50 mg/liter of standard L-amino acids (excluding methionine), 100 nM vitamin B₁₂, and trace elements (44). Expression was induced with 0.5 mM IPTG (isopropyl-β-D-thiogalactopyranoside) at 16°C for 12 h. Cells were then harvested and resuspended in lysis buffer containing 50 mM Tris (pH 8.0), 50 mM NaCl, 1 mM dithiothreitol (DTT), 10 mM MgCl₂, 20 μg/ml DNase, and 1× protease inhibitor cocktail V (EMD Biosciences). The cells were disrupted in a BeadBeater (Biospec) using 0.1-mm-diameter glass beads. Cellular debris was cleared from the lysate by spinning at 27,200 × g for 2 h. The supernatant was then filtered and loaded onto a Blue Sepharose column (GE Healthcare) that had been equilibrated in a mixture of 50 mM Tris (pH 8.0), 50 mM NaCl, and 1 mM DTT. Protein collected from the flowthrough was further purified by anion-exchange chromatography using a HiTrap Q high-performance (HP) column (GE Healthcare). The purified protein was dialyzed overnight against buffer containing 50 mM Tris (pH 8.0), 50 mM NaCl, and 1 mM DTT and was then concentrated to 10 mg/ml using a Centrprep centrifugal concentrator (Milipore) and flash frozen until further use.

Crystallization. Purified protein was crystallized in 20% polyethylene glycol 8000 (PEG 8000), 0.1 M Tris (pH 8.0), 0.2 M NaCl, 3% ethylene glycol, and 8 mM 3-[(3-cholamidopropyl)dimethylammonio]-1-propanesulfonate (CHAPS). Wells were set up using sitting-drop vapor diffusion at 21°C, with drops consisting of 2 parts buffer and one part protein. Crystals grew to 100 μm within 3 to 4 days. Perfluoropolyether (Hampton Research) was used as a cryo-protectant. The protein crystallized in space group P2₁ with the unit cell parameters $a = 39$, $b = 165$, $c = 67$ Å, and $\beta = 97^\circ$. The corresponding unit cell volume can accommodate a single molecule in the asymmetric unit.

Crystal dehydration. A crystal dehydration method was developed that significantly improved the mosaic spread and diffraction power of the crystals (45). Both the well and drop solution were replaced with mother liquor that had a 3 to 5% increase in precipitant concentration. Crystals were left to dehydrate for a minimum of 48 h before making another incremental increase in the precipitant. Successfully dehydrated crystals had a reduced b unit cell parameter of up to 15 Å, with the largest difference resulting in a 10.5% decrease in the unit cell volume. The crystal that produced the best diffraction data and led to structure solution had only a 3-Å difference in the b unit cell parameter.

Data collection, structure determination, and refinement. The structure was solved by single-wavelength anomalous dispersion (SAD) using a selenomethionine (SeMet) derivative (46). Anomalous diffraction data were collected at beamline 23-ID of the GM/CA-CAT facilities of the Advanced Photon Source, Argonne National Laboratory. Crystals were partitioned using the 10-μm minibeam (47). This prevented global-scale radiation exposure and allowed for more data to be collected from a single crystal. The data were processed and reduced using the HKL2000 software package (48). The locations of 3 Se sites were found using SHELX C/D and were used as a starting point for locating additional sites in autoSHARP (49, 50). The resulting experimental phases extended to a 3.8-Å resolution and produced an electron density map in which approximately 60% of the backbone could be placed in NBD1, NBD2, and parts of the HSD. Model building was performed in Coot (51). The phases from the partial model were then combined with the experimental phases using SigmaA and used as a starting point for progressive runs of density mod-

ification in DM (52, 53). This facilitated the placement of the backbone in the PPXD as well as in other parts of the model. Initially, sequence was assigned by the positions of the Se atoms and from the density of large side chains. Then a real-space cross-validation procedure called “ping-pong” cross-validation was used to complete the structure (54). Briefly, the model was split into two sets. Side chains that could be identified in the first set of residues were used during phase combination and density modification. The resulting map was used to place side chains for the second set of residues, and the process continued in alternation. Structure refinement was carried out in autoBuster (55).

Suppressor screen and reconstruction. Spontaneous suppressors of the *secA2*^{K129R} strain were isolated by plating onto Mueller-Hinton agar at 37°C, as described previously (30). The *secA2*^{K129R} strain has the chromosomal *secA2* gene deleted and carries a copy of the *secA2* gene encoding *secA2*^{K129R} integrated at the chromosomal L5 *att* site. The *secA2*^{K129R} gene of the suppressors was PCR amplified and sequenced to identify intragenic suppressor mutations. To confirm that suppressor phenotypes were due to sequenced mutations in *secA2*^{K129R}, the intragenic suppressors were recreated in a fresh strain background. PCR-amplified *secA2*^{K129R} gene products from the intragenic suppressors were subcloned into pCR2.1 followed by cloning into pMV306. The resulting vectors were electroporated into the Δ*secA2* mutant of *M. smegmatis*, and transformants were tested for sensitivity to sodium azide and SecA2 localization.

Azide sensitivity assay. Cultures were plated for sensitivity to sodium azide as previously described (29). In brief, 200 μl of saturated (optical density at 600 nm [OD₆₀₀] of 2.0) *M. smegmatis* culture was mixed with 3.5 ml of molten 7H9 top agar and then poured onto a 7H10 bottom agar plate lacking Tween. Sterile 6-mm-diameter filter discs were placed onto the surface of the cooled top agar. Ten microliters of 0.15 M sodium azide was then added to the disc. The plates were incubated for 2 days at 37°C, and the resulting zones of growth inhibition were measured. Each strain was tested in triplicate.

Subcellular fractionation and immunoblotting. To determine the subcellular localization of SecA2 in *M. smegmatis*, we fractionated bacterial whole-cell lysates as described previously (22, 29). Whole-cell lysates were generated by five passages through a French pressure cell. The lysates were separated into cell envelope (100,000 × g pellet) and soluble (100,000 × g supernatant) fractions. Protein derived from the same amount of starting cells for each fraction was analyzed by SDS-PAGE and immunoblots using an anti-SecA2 antibody at a 1:20,000 dilution (56). For quantification, secondary antibody conjugated to alkaline phosphatase was used and detected using the ECF reagent (GE Healthcare). Fluorescence was quantified using a phosphorimager and ImageQuant 5.2 (Molecular Dynamics).

Protein structure accession number. The structural coordinates of the *MtbSecA2* model used in this study have been deposited in the Protein Data Bank under identification no. 4UAQ.

RESULTS

Crystal structure of *MtbSecA2*. *MtbSecA2* (Rv1821) was crystallized in space group P2₁, and the structure was solved by single-wavelength anomalous dispersion (SAD) (57) to a resolution of 2.8 Å. The asymmetric unit of the crystal contains a single monomer, and there is no indication of a higher-order oligomer in the crystal lattice. A total of 705 out of 778 residues of the apoprotein were visible in the electron density and could be built. The crystallographic statistics are shown in Table 1.

Broad structural similarity between *MtbSecA1* and *MtbSecA2*. The tertiary structure of SecA2 is very similar overall to those of *MtbSecA1* and other orthologs in the SecA family (Fig. 1). SecA2 has a long 65-Å (45-amino-acid) helix scaffold domain (HSD), which interconnects four other domains, including two nucleotide-binding domains (NBD1 and NBD2), the IRA1 domain, and the PPXD domain. NBD1 and NBD2 pack together to form a

TABLE 1 Data collection and refinement statistics for SAD (SeMet) structure of SecA2

Parameter	Value(s) for SecA2 ^a
Data collection	
Space group	P2 ₁
Cell dimensions	
<i>a</i> , <i>b</i> , <i>c</i> (Å)	39.60, 162.09, 67.31
α , β , γ (°)	90.00, 95.87, 90.00
Wavelength (Å)	0.97949
Resolution (Å)	35.64–2.8 (2.85–2.8)
<i>R</i> _{sym} or <i>R</i> _{merge} (%)	0.096 (0.171)
Avg <i>I</i> / σ (<i>I</i>) ^c	24.3 (1.4)
Completeness (%)	0.72 (0.168)
Redundancy	4.1 (1.9)
Refinement	
Resolution (Å)	2.8
No. of reflections	16,255
<i>R</i> _{work} / <i>R</i> _{free}	0.291 (0.212)
No. of atoms	
Protein	4,894
Water	67
<i>B</i> -factors	
Protein	85.2
Water	58.3
RMSD ^b	
Bond length (Å)	0.01
Bond angle (°)	1.26

^a Values in parentheses are for the highest-resolution shell.

^b RMSD, root mean square deviation.

^c *I*, intensity of a reflection.

DEAD box motor domain with an ATP-binding site between them. Catalytically important residues, such as K115 and R545 are conserved (see Fig. S1 in the supplemental material), consistent with demonstrated ATPase activity of SecA2 (28). As in other SecA

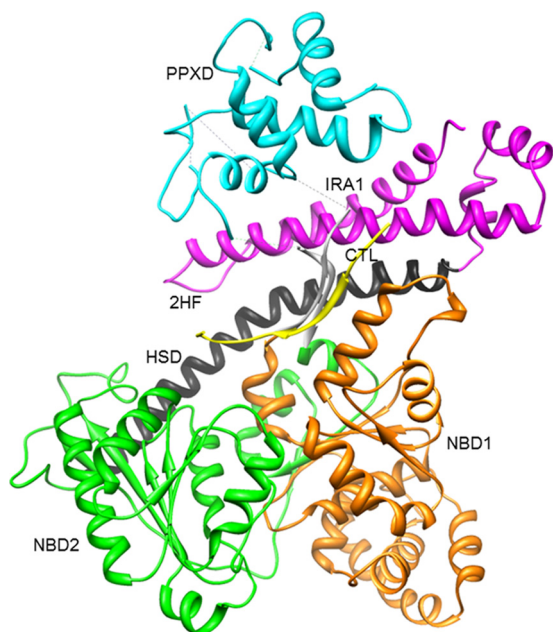


FIG 1 Domain architecture of *MtbSecA2*. Orange, NBD1; green, NBD2; cyan, PPXD; magenta, IRA1; black, HSD; yellow, C-terminal linker (CTL).

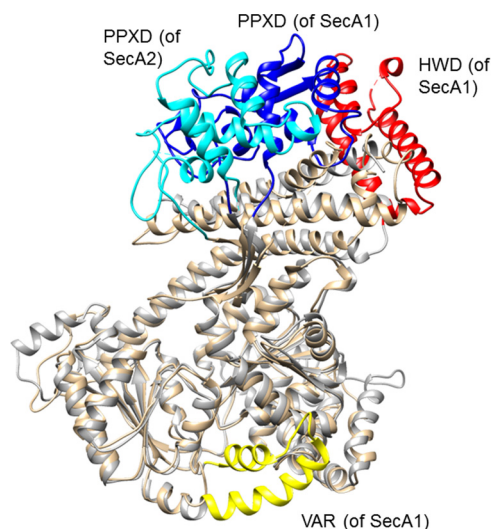


FIG 2 Comparison of *MtbSecA2* with *MtbSecA1*. Relative to SecA1 (gray backbone) (PDB code 1NL3), SecA2 (tan backbone) is smaller, lacking the HWD (red) and the VAR domain (yellow). Also, the PPXD domain has undergone rotation (SecA1 [blue] → SecA2 [cyan]).

structures, the IRA1 domain consists of a pair of alpha-helices packed in parallel to the HSD (forming a 3-helix bundle) and connected by a 9-aa loop (known as the 2-helix finger [2HF]). SecA2 lacks the ~70-aa C-terminal domain (CTD) that is present in SecA1 orthologs. However, the short linker to this domain, called the C-terminal linker (CTL [residues 734 to 778]), is retained in the SecA2 sequence. The CTL is largely disordered in the crystal structure. However, as observed in previous SecA structures (33), part of the CTL of SecA2 (residues 749 to 759, shown in yellow in Fig. 1) forms a third β -strand along the outside the preprotein binding site. Note that this region is preceded by a disordered loop (residues 734 to 748), which appears as a discontinuity between IRA1 and CTL in the figure, and followed by only 19 residues to the C terminus, which are also disordered. During model building, sequence assignment in this strand was aided by the location of SeMet757 and the density of bulky side chains, which helped to rule out the possibility of a bound preprotein substrate.

Differences between the structures of *MtbSecA1* and *MtbSecA2*. Despite the overall similarity between the structures of SecA1 and SecA2, there are several notable differences. One structural difference between SecA1 and SecA2 is found in the nucleotide-binding region. SecA2 lacks the VAR domain (58), which in other SecA orthologs consists of a pair of helices that reach out from NBD2 and cover over the ATP-binding site (Fig. 2). Consequently, the ATP binding site is more solvent exposed in SecA2. The VAR domain is present in some SecA orthologs, including *MtbSecA1* (31) and *E. coli* SecA (32), but it is absent in others, such as *B. subtilis* SecA (33) and *T. maritima* SecA (*TmSecA*) (39). The functional significance of the absence of the VAR domain in SecA2 is unknown.

A second structural difference involves the orientation of the PPXD domain. As in other SecA structures, the PPXD domain consists of an $\alpha + \beta$ -fold that is attached to the NBD1 motor domain by a pair of anti-parallel β -strands that cross over the HSD. The PPXD of *M. tuberculosis* SecA2 occupies a distinct orientation

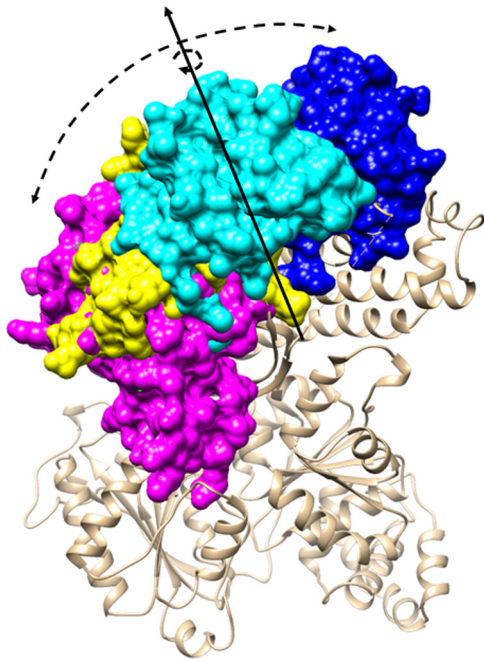


FIG 3 Comparison of different orientations of the PPXD domain. Shown are *MtbSecA2* (cyan), *MtbSecA1* (PDB code 1NL3) (dark blue), *B. subtilis* SecA (PDB code 1TF2) (yellow), and the *TmSecA*-SecYEG complex (PDB code 3DIN) (red). All four PPXD domains are superposed onto the body of *MtbSecA2* (orange). At one extreme, in the *MtbSecA1* structure (right, dark blue), the PPXD is packed against the HWD (missing in SecA2), representing the signal peptide-recognition site closed conformation. At the other extreme (left, red), the PPXD from the *T. maritima* complex with SecYEG represents the “preprotein clamp closed” configuration, where contact is made with NBD2 (orange, lower left). The *MtbSecA2* PPXD occupies a unique intermediate position (cyan).

compared to previous SecA structures, as illustrated in Fig. 3. The PPXD in previous SecA structures had been observed in several different orientations, ranging from contact with the HWD (to form a “signal peptide binding-cleft closed” conformation, as observed in 1nl3) to contact with NBD2 (to form a “preprotein clamp closed” conformation, as observed in PDB code 3DIN) (38, 59) produced by a rigid-body rotation relative to the rest of the protein (38, 39). The PPXD in SecA2 occupies an intermediate position between these two extremes.

The most striking structural difference in SecA2 is that the HWD is missing (Fig. 2) due to deletion of 70 aa that form a helical domain at the end of the HSD, as anticipated from the sequence alignment (see Fig. S2 in the supplemental material). In SecA2, the remaining 23 residues connect the HSD directly to IRA1, bypassing the helical wing domain. In other SecA structures, including *MtbSecA1*, the body of the HWD forms a deep hydrophobic cleft with PPXD, which can open or close against it (39), with the signal peptide binding site at the base (formed by residues from PPXD and IRA1) (39, 40). The absence of the HWD in SecA2 makes the cleft significantly more open and solvent exposed (illustrated in Fig. S3 in the supplemental material), which could help SecA2 recognize its unique substrates that are distinguished by features of their mature domains—possibly a tendency to fold prior to export (23).

The functionally important two-helix finger (2HF), which is a 9-residue loop connecting two helices in the IRA1 domain that

TABLE 2 Conservation of the 2HF among SecA homologs

Species	Protein	Sequence ^a
<i>E. coli</i>	SecA1	LRGYA <u>Q</u> KD <u>P</u>
<i>T. maritima</i>	SecA1	LRSYGQK <u>D</u> P
<i>M. tuberculosis</i>	SecA1	LRAMAQ <u>R</u> D <u>P</u>
<i>M. smegmatis</i>	SecA1	LRAMAQ <u>R</u> D <u>P</u>
<i>M. tuberculosis</i>	SecA2	LRAL <u>G</u> RQ <u>N</u> P
<i>M. avium</i>	SecA2	LRAL <u>G</u> RQ <u>N</u> P
<i>M. smegmatis</i>	SecA2	LRAL <u>G</u> RQ <u>N</u> P
<i>S. aureus</i>	SecA2	LRSYAQQ <u>N</u> P
<i>L. monocytogenes</i>	SecA2	LRAYGQID <u>P</u>
<i>S. gordonii</i>	SecA2	LRGYAQN <u>N</u> P
<i>C. difficile</i>	SecA2	LKSYA <u>Q</u> KD <u>P</u>
<i>C. glutamicum</i>	SecA2	LRAL <u>I</u> ARE <u>T</u> P

^a Key residues are underlined.

inserts into the SecYEG pore, is conserved in the *MtbSecA2* structure (residues 695 to 703) (Table 2). However, the 2HF loop in *MtbSecA2* adopts a different three-dimensional conformation compared to previous structures. In the *MtbSecA2* structure, the 2HF is observed to close down approximately 10 Å onto the HSD, like a jaw hinge (Fig. 4), due to differences in how the ends of the helices unwind (even though the 2HF amino acid sequence itself is highly conserved, as shown in Table 2). This orientation contrasts with the conformation observed in most other SecA structures, in which the loop is more flipped out into solvent (Fig. 4); however, the conformations of the 2HF loop are also quite variable among SecA crystal structures (see Fig. S4 in the supplemental material). Fluorescence studies also suggest that the 2HF loop is flexible and can adopt different conformations in solution (37).

Similarities between SecYEG binding regions of *M. tuberculosis* SecA1 and SecA2. The conservation of the overall structure of SecA2 is consistent with a model in which SecA2 works with SecYEG to translocate SecA2-dependent proteins across the membrane. Furthermore, the key regions of SecA2 that would interact with the SecYEG pore are conserved, including the 2HF. The helix-terminating proline in the 2HF is present in SecA2 (Pro703), as it is in all SecA homologs (Table 2). Tyr794 in *E. coli*

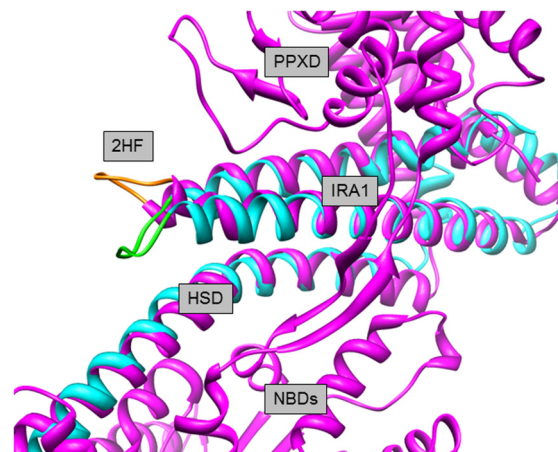


FIG 4 Conformation of the two-helix finger (2HF). The HSD of *MtbSecA2* (cyan) is shown superposed on the apo structure of *MtbSecA1* (purple). The loops connecting the two helices are shown in orange (SecA1) and green (SecA2).

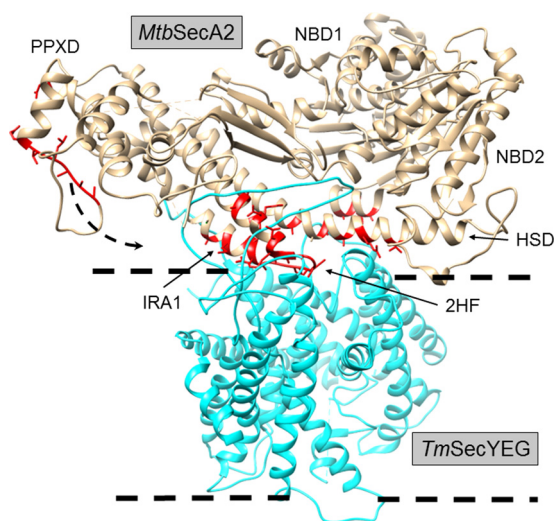


FIG 5 Interface residues (red) of *MtbSecA2* (tan) that would contact SecYEG (cyan), based on superposition with *TmSecA* (PDB code 3DIN). Note that the red residues highlighted in the PPXD correspond to residues of *TmSecA* that contact SecYEG as its PPXD is rotated into contact with SecYEG.

SecA is another critical residue in the 2HF (36). Although it is substituted for by Leu698 in *MtbSecA2*, this tyrosine is substituted by large hydrophobic residues in 20% of SecA homologs (methionine in *MtbSecA1*). Furthermore, structural data from the *TmSecA*-SecYEG complex supports that hydrophobic substitutions, such as leucine, can be accommodated at this position, as the side chain sits in a hydrophobic pocket in SecY (34).

Structural superposition of *MtbSecA2* onto *TmSecA* in the *TmSecA*-SecYEG complex (PDB code 3DIN [34]) (Fig. 5; see Fig. S5 in the supplemental material) further indicates that SecA2 preserves many of the structural features of SecA implicated in binding to SecYEG. This includes amino acids in the *MtbSecA2* 2HF and immediately adjacent regions of IRA1 that contact SecY in the *TmSecA*-SecYEG complex (aa 687 to 715 in SecA2) (Table 3 and Fig. 5). There are also regions of NBD2 and the HSD that are structurally conserved in the SecA2 structure and positioned for contact with SecY (Table 3 and Fig. 5). These residues in NBD2, IRA1, and the HSD are clustered at the interface with SecY. In addition, although the PPXD of SecA2 is rotated away and does not appear to make direct contact with SecY in the superposition, if it were rotated into an orientation similar to that observed in *TmSecA* in the complex, it would place additional SecA2 residues (listed in Table 3) in contact with SecY, as shown in Fig. 5. It is notable that *MtbSecA2* D607 (in the HSD) corresponds to one of the residues in *E. coli* SecA (position 640) that can be cross-linked with SecY using photoactivatable unnatural amino acids (60).

Mapping of suppressor mutations on the SecA2 structure. Prior studies indicate that a SecA2 dominant-negative protein with an amino acid substitution in the ATP binding Walker box, making it unable to bind ATP, is locked in a nonfunctional complex, likely with SecYEG, at the membrane (29). In order to identify important residues in SecA2, we identified intragenic suppressor mutations that could overcome the *secA2* dominant-negative phenotypes (30) with the rationale being that such mutations might map to sites of protein interactions in SecA2 complexes. For convenience, these experiments were performed with the *M.*

smegmatis ortholog of SecA2, which has 83% amino acid identity to *MtbSecA2* and is able to substitute for the *MtbSecA2* in cross-species complementation experiments (29). An *M. smegmatis* strain expressing the dominant-negative *MsSecA2*^{K129R}, which has an amino acid substitution in the Walker box (equivalent to K115 in *MtbSecA2*) was used. All suppressors identified reversed the severe dominant-negative phenotypes caused by SecA2^{K129R}, as assessed by azide sensitivity assays (5) and colony size on rich agar (30) (Fig. 6 and data not shown), but they still exhibited a phenotype similar to that of a Δ *secA2* null mutant.

Eight independent suppressors with mutations in the coding sequence of *secA2*^{K129R} were identified by sequencing, mapping to four different domains: NBD1, NBD2, PPXD, and IRA1 (Table 4). All eight suppressor mutants produced full-length SecA2 protein at normal levels, as confirmed by Western blot analysis. Each mutation was validated to be responsible for the suppression by re-testing the phenotype of individual mutations when introduced into a fresh *secA2*^{K129R} mutant background (Fig. 6).

When mapped to the SecA2 structure, all of the suppressor mutations were located on the surface of the protein (Fig. 7). For simplicity, below we will refer to the suppressors using amino acid numbering that corresponds to *MtbSecA2* (Table 4). There were three categories of suppressors. The first set of suppressor mutations affected the same surface loop of NBD1. There were two suppressors derived from independent cultures with identical mutations in NBD1 and a third suppressor with a different mutational alteration that mapped to the same site in NBD1. These NBD1 suppressors involve a 4-residue loop, ¹⁶⁸STPD¹⁷², in *M. tuberculosis* connecting a β -strand and an α -helix; this loop was deleted in one mutant and duplicated in another. It is currently unknown what role these residues play, but it is striking that three out of eight suppressor mutations involved this surface-localized loop of the nucleotide binding domain, suggesting it is a functionally important point of contact for SecA2.

The second group of suppressors (three in total) clustered in the SecA “polypeptide clamp” region made up of PPXD and NBD2 domains. Two suppressor mutations mapped to the SecA2 PPXD domain: a nonsynonymous substitution, D316H, and an insertion of a second glutamate at E354. These amino acids are in separate loops in the PPXD domain, but they are proximal in the three-dimensional structure, approximately 7 Å apart (Fig. 7a). The PPXD is positioned far from the NBD2 domain in the SecA2 structure. (The distance between the closest residues of the two domains is 23 Å, representing a “clamp open” state.) However, in the *TmSecA*-SecYEG complex, the corresponding PPXD loops to which these suppressor mutations map come in contact with NBD2. Moreover, the *TmSecA* residue corresponding to the D316H suppressor in the *MtbSecA2* PPXD is in direct contact

TABLE 3 Residues of *MtbSecA2* predicted to be in contact with SecY based on structural superposition with *TmSecA* in complex with SecYEG (PDB code 3DIN)

Domain	<i>MtbSecA2</i> residues predicted to contact SecY
NBD1	None
NBD2	E392, R395, Q396
HSD	V600, R604, D607, A610, R614
IRA1	Most residues spanning 687–715 (including residues of the 2HF and surrounding IRA1 helices)
PPXD	N270, H272, T274, E275, D289

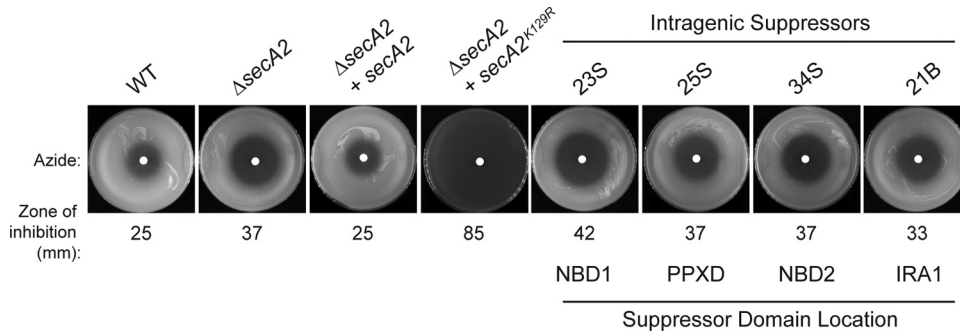


FIG 6 Intragenic suppressors suppress the azide sensitivity phenotype of $secA2^{K129R}$. Lawns of the indicated strains were plated and tested for sensitivity to 10 μ l of 0.15 M sodium azide (applied to a paper disk in the center of the plate) for 2 days at 37°C. Average inhibition was calculated by measuring the diameter of the zone of azide inhibition, and values are the means of three biological replicates. The $\Delta secA2$ mutant *M. smegmatis* strain was transformed with plasmids containing either $secA2$, $secA2^{K129R}$, or a reconstructed intragenic suppressor with the $secA2^{K129R}$ mutation in combination with an intragenic suppressor mutation located in one of the following domains: NBD1, NBD2, PPXD, or IRA1.

with NBD2 in the *TmSecA*-SecYEG complex (34) (Fig. 7b). It should be noted that this *TmSecA* complex with SecYEG represents an extreme conformation (induced by ADP and BeFx in the crystallization buffer) in which the preprotein channel is entirely collapsed (i.e., a loop of the PPXD actually inserts into the preprotein binding channel). In a structure of SecA bound to a preprotein substrate (PDB code 3JV2 [61]), the PPXD does not rotate quite as far toward NBD2 as in the SecA-SecYEG complex, but the residues corresponding to the suppressor mutations are still on the surface of the PPXD in a region that would be in position to interact with SecYEG or the lipid bilayer (similar to the red residues highlighted in Fig. 5). Thus, these suppressor mutations could disrupt intramolecular interactions when the PPXD rotates to form the “clamp” around the translocating polypeptide (41) or could lock it in the extreme closed state such that the preprotein channel is collapsed altogether. Strikingly, the NBD2 suppressor T449I in *M. tuberculosis* also maps to the SecA “preprotein clamp” region and is proximal (within 10 Å) to the two PPXD suppressor mutations when the clamp is closed (based on the analogous residues in the *TmSecA*-SecYEG docked structure [34]) (Fig. 7). Thus, these three suppressors in NBD2 and PPXD could conceivably cause a defect in clamp closure during translocation. In light of past studies suggesting that interactions between $SecA2^{K129R}$ and SecYEG are responsible for the dominant-negative phenotype (30), these results suggest that a defect in clamp closure may dislodge or prevent SecA2 interactions with SecYEG by disrupting interactions with the polypeptide being translocated through the channel.

The final group of intragenic suppressors identified have deletions in IRA1. One suppressor has a deletion of residues 714 to 721 in *M. tuberculosis*, and another suppressor has a very similar, yet distinct, deletion of residues 712 to 719 in *M. tuberculosis*. These deletions are in the middle of one of the α -helices, just downstream from the 2HF that forms part of the interface with SecYEG (Fig. 5 and 7 and Table 3), and similar mutations in IRA1 have previously been shown to disrupt binding to SecYEG (62). Furthermore, one of the deleted residues in both of the IRA1 suppressors is Phe715, which is a conserved residue predicted to contact SecY (colored red in Fig. 5) that is equivalent to the highly conserved Phe798 (in *TmSecA*). In the *TmSecA*-SecYEG structure, Phe798 (in *TmSecA*) forms an aromatic stacking interaction with Tyr418 in the C-terminal tail of *TmSecY* (34). This interaction

appears to be crucial to docking as the equivalent tyrosine residue in *E. coli* SecY (Tyr429) is the location of a cold-sensitive mutation that prevented insertion of SecA into the membrane channel (63). These interacting residues are highly conserved in all Sec systems, including *MtbSecA2* (Phe715) and *MtbSecY* (Tyr436). The fact that this group of intragenic $secA2$ suppressor mutants harbors deletions in a structurally conserved and critical SecY-interacting region of IRA1 (Fig. 5 and Table 3) is consistent with their mode of suppression being avoidance of complex formation between $SecA2^{K129R}$ and SecYEG.

Intragenic suppressors alter membrane localization of the dominant-negative SecA2. In the wild type, *MsSecA2* is predominantly found in the soluble cytoplasm-containing fraction. In contrast, the localization of $SecA2^{K129R}$ is almost exclusively in the membrane-containing cell envelope pellet (29) (Fig. 8). This is consistent with a model for $SecA2^{K129R}$ being locked in a protein complex with SecYEG at the membrane. Since we predicted that some of the intragenic suppressors alleviate SecYEG interactions, we determined the membrane localization of $SecA2^{K129R}$ in the intragenic suppressor mutant background. Strains were lysed and then fractionated into cell envelope (pellet) and soluble (cytoplasmic) fractions. Western blot analysis with anti-SecA2 antibodies on fractions was then carried out to localize the protein. In each of the representative intragenic suppressors analyzed, the distribution of $SecA2^{K129R}$ shifted from the envelope, as seen in the starting $secA2^{K129R}$ strain, to the soluble cytoplasmic fraction (Fig. 8). Suppressor mutations in the “clamp” (PPXD and NBD2) and IRA1 domains had the most dramatic effects, restoring partition-

TABLE 4 Suppressor mutations observed in *M. smegmatis* $SecA2^{K129R}$

Isolate(s) ^a	Effect on residue(s) in <i>MsSecA2</i>	Domain	Corresponding residue(s) in <i>MtbSecA2</i>
6S, 9S	Deletion of residues 182–185	NBD1	168–171 (STPD)
23S*	Duplication of residues 182–185	NBD1	168–171
2S	Asp326→His	PPXD	D316
25S*	Glu insertion at residue 364	PPXD	E354
34S*	Thr459→Ile	NBD2	T449
21B*	Deletion of residues 734–741	IRA1	714–721
38S	Deletion of residues 732–739	IRA1	712–719

^a An asterisk indicates the suppressor was subcloned and retested in *M. smegmatis*.

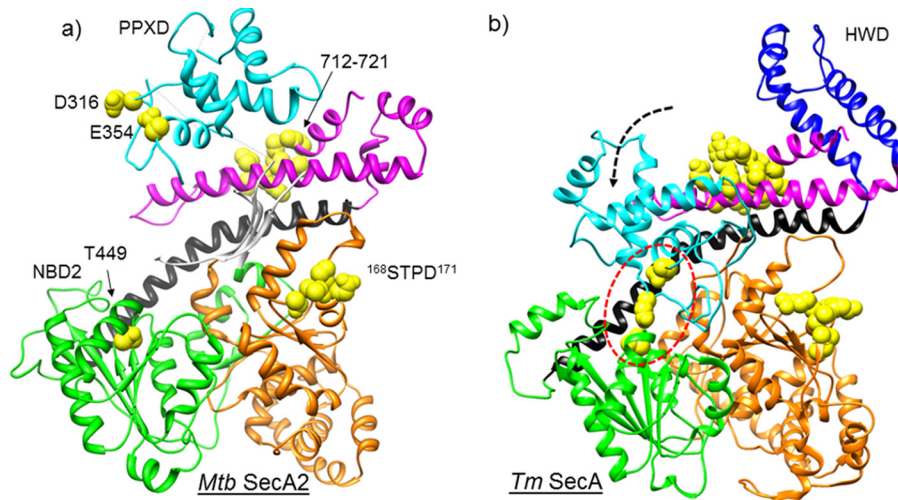


FIG 7 (a) Suppressor mutations from *MsSecA2*^{K129R} mapped onto *MtbSecA2*. Mutations are shown as yellow spheres. (b) Suppressor mutations mapped onto the *TmSecA* complex with SecYEG (PDB code 3DIN). In the complex with SecYEG, SecA is in the “preprotein clamp closed” conformation, in which PPXD (cyan) is swung down (arrow) to make contact with NBD2 (green). In this conformation, the residues affected by the suppressor mutations in the PPXD and NBD2 domains can be seen to come into contact (circled).

ing of SecA2 between the cell envelope and cytoplasm to almost wild-type levels. These data support a model in which the intragenic suppressor mutations alleviate the dominant-negative phenotype by disrupting protein-protein interactions involving the SecYEG membrane complex and/or the translocating polypeptide.

DISCUSSION

Over 30 years ago, SecA was identified as a critical component of the protein export system of bacteria (64). Since that time, there have been extensive genetic, molecular, biochemical, biophysical, and structural studies to understand SecA function. Of the two SecAs in *M. tuberculosis*, SecA1 is the counterpart of the well-studied canonical SecA, while SecA2 has a distinct function from SecA1 and a nonoverlapping substrate specificity profile. The structure of *MtbSecA2* we report is the first structure of any SecA2 protein. The broad structural similarity observed between the two solved *MtbSecA* structures indicates that, even after decades of mechanistic studies, gaps in our understanding of SecA proteins remain.

The smaller size of SecA2 versus SecA1 and canonical SecA proteins appears to come from the absence of the HWD, the VAR domain, and a C-terminal domain (CTD [although it still retains the CTL linker]) reducing the overall size of the protein product from 949 aa to 778 aa (see Fig. S2 in the supplemental material). The lack of an HWD is the most striking structural difference in SecA2. Without the HWD, the signal peptide recognition site of SecA2 is more solvent exposed and thus more accessible to protein substrates. This structural difference may help explain the ability of SecA2 to export substrates with distinctive features of their mature domain, possibly a propensity to fold prior to export (23). The “open” nature of the cleft created by the absence of a HWD could provide a broad surface against which folded proteins could possibly dock and unfold for translocation through the SecYEG transmembrane pore. Several pieces of experimental evidence support the possibility that the HWD could interact with preproteins. While a nuclear magnetic resonance (NMR) structure of

SecA bound to a signal peptide did not identify any residues of the HWD that directly interact with the signal peptide (40), several residues of the HWD were found to form cysteine-based cross-links with a synthetic signal peptide (42), which may result from transient states (i.e., alternative conformations of the HWD) sampled dynamically in solution. In fact, the HWD is observed to rotate by up to 15° between different crystal structures, depending on the oligomeric state (39). This suggests the HWD itself is mobile in solution, which is supported by fluorescence-based (flu-

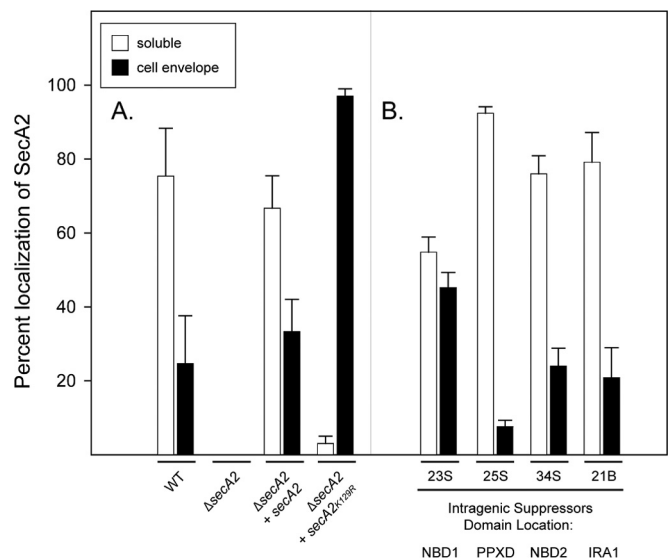


FIG 8 Subcellular localization of SecA2 is altered in intragenic suppressors of *secA2*^{K129R}. Whole-cell lysates of the indicated strains were fractionated into a cytoplasm-containing soluble fraction and membrane-containing cell envelope fraction. Representative intragenic suppressors (PPXD, NBD2, IRA1, and NBD1) are indicated. Protein derived from an equal number of cells was analyzed by SDS-PAGE, and quantitative immunoblot analysis with anti-SecA2 antibodies was performed. The percentage of localization in a given fraction is plotted. Error bars represent the means from three independent replicates.

rescence resonance energy transfer [FRET]) studies (65). Furthermore, the mobility of the HWD appears to be influenced by the presence of a preprotein (66). Thus, the absence of the HWD in SecA2 could potentially affect substrate recognition. The 70-residue deletion of the HWD observed in *MtbSecA2* is a general feature among actinomycetes (including *Mycobacterium* and *Corynebacterium* species) (see Fig. S2 in the supplemental material). It should be noted that other Gram-positive SecA2 proteins also appear to have a truncated version of this domain (deletions of 13 to 18 residues for *Streptococcus gordonii* and *L. monocytogenes*, respectively). Until structures of these other SecA2 orthologs are solved, the potential consequences of these HWD truncations remain unknown. It is possible that a reduced HWD could open up the signal peptide binding cleft and/or increase the site of interaction with preproteins, as we propose for *MtbSecA2*. To achieve a complete picture of SecA2 function going forward, the consequences of a truncated or deleted HWD will need to be explored in both mycobacterial and Gram-positive SecA2 proteins.

The significance of the absence of the VAR domain in the SecA2 NBD region is less clear. The lack of the VAR domain leaves the nucleotide-binding site relatively solvent exposed. While other SecA2 orthologs also lack the VAR domain (see Fig. S2 in the supplemental material), one-third of bacterial SecA (1) proteins lack this domain as well (58). In *E. coli* SecA, the VAR domain has been shown to regulate ATPase activity and ADP release, as *secA* Δ var mutants display higher ATPase activity and faster ADP release rates (58). However, *MtbSecA2* (28) was recently reported to release ADP more slowly (not more quickly) than the VAR-containing *MtbSecA1* (67).

Mycobacterial SecA2 proteins, as well as SecA2s in many other organisms, lack the C-terminal domain (CTD) (see Fig. S2 in the supplemental material). The CTD in SecA1 proteins consists of a tail of ~70 aa that is disordered in all previous crystal structures (1). In most bacteria, the CTD of SecA contains a Zn²⁺ finger domain that binds to the protein export chaperone SecB (68). Mycobacteria are an exception, in that the CTD of SecA1 does not contain the conserved cysteines of a Zn²⁺ finger motif. However, this may not be too surprising because, like Gram-positive bacteria (69), no SecB ortholog with a function in protein export has so far been identified in mycobacteria. Thus, because of the lack of Zn²⁺ finger motif in the CTD of SecA1 and lack of a SecB ortholog, the absence of a CTD in *MtbSecA2* seems unlikely to be a significant contributing factor to the unique function of SecA2.

In comparison to all prior SecA structures, the SecA2 structure also revealed new orientations of the PPXD and the 2HF loop. However, these differences probably reflect the conformational plasticity of these two structural elements. Given the mobility of the PPXD domain already established for canonical SecA proteins, it seems likely that the PPXD orientation observed in SecA2 represents a previously unobserved structural intermediate in the transition of the preprotein binding clamp from the open to closed position (38). The unique orientation of the 2HF loop observed in SecA2, which occurs at a key point of interaction with the translocation channel and varies considerably among SecA structures, is probably a consequence of the flexibility of this loop in solution.

Given that there is no corresponding SecY2 partner in the *M. tuberculosis* genome, an important mechanistic question to be answered is whether SecA2 works with the canonical SecYEG channel to export proteins. In prior studies, we described a dominant-

negative *secA2* mutation that exhibits more severe phenotypes than a Δ *secA2* deletion mutant (29). Such phenotypes often result from a dominant-negative protein being locked in a nonproductive complex with its normal binding partners. Furthermore, we showed extragenic suppressors that overexpress SecY suppress the *secA2*^{K129R} dominant-negative phenotype, which argues for an interaction between SecA2^{K129R} and SecY (30). Here, we identified intragenic suppressors of *secA2*^{K129R}, and all of them mapped to the surface of the SecA2 structure. One group of suppressors mapped to the IRA1 domain of SecA2 in regions where similar mutations disrupt *E. coli* SecA binding to SecYEG (62). These IRA1 suppressors also restored cytoplasmic localization of SecA2^{K129R}. These results can be explained by the IRA1 suppressor mutations preventing SecA2^{K129R} interactions at the membrane SecYEG channel, and they support the model for SecA2 working with SecY to promote export of its specific substrates. The suppressors that mapped to the “polypeptide clamp” region of SecA2 could similarly suppress the dominant-negative phenotype. However, in this case, the suppression would result from the inability of SecA2 to trap the translocating polypeptide in the center of the SecYEG channel, causing SecA2 to fail to engage SecYEG (without the substrate) or causing the ternary system (SecYEG-SecA2-preprotein) to dissociate.

The SecA structure reported here is of a monomer. In other studies, SecA proteins have been crystallized as monomers (54) or dimers (39), and the issue of the oligomeric state of SecA during protein translocation has remained controversial (37, 70–72). A recent study demonstrated the ability of recombinant *MtbSecA1* and *MtbSecA2* to physically interact *in vitro* (73). If SecA1-SecA2 heterodimers form, it is possible that interactions between SecA1 and SecY avoid the need of SecA2 to directly interact with SecY. However, it is currently unclear if SecA1-SecA2 dimers exist and/or are functional in mycobacteria. Furthermore, the dominant-negative SecA2 phenotypes and the intragenic suppressors reported here, combined with structural conservation of SecA-SecY contact sites in SecA2, argue for the ability of SecA2 and SecY to interact. Ultimately, to clarify the mechanistic details of SecA2-dependent protein export, it will be necessary to study the pathway with an *in vitro* reconstitution system, as was used to dissect the mechanistic details of the *E. coli* Sec pathway.

Since the SecYEG channel requires that proteins be unfolded for translocation (25), the possibility of SecA2 working with the SecYEG channel is intriguing, in light of experiments suggesting that SecA2 substrates are distinguished by a tendency to fold in the cytoplasm (23). The role of SecA2 could be to promote recognition of proteins that would normally be overlooked by the canonical SecA1-SecYEG translocase or to help maintain proteins in an unfolded state prior to or during export. The regions of structural difference and suppressor mutations identified in this study represent exciting new directions for exploring the functional differences between SecA2 and SecA1 proteins.

ACKNOWLEDGMENTS

This work was supported by National Institutes of Health NIAID AI054540 (M.B.), NIH P01 AI095208 (J.C.S.), and A0015 (J.C.S.) from the Robert A. Welch Foundation.

We thank Satheesh K. Palaninathan for suggestions on a preliminary version of the manuscript.

FUNDING INFORMATION

Robert A. Welch Foundation provided funding to James C. Sacchettini under grant number A0015. HHS | NIH | National Institute of Allergy and Infectious Diseases (NIAID) provided funding to James C. Sacchettini under grant number AIO95208. HHS | NIH | National Institute of Allergy and Infectious Diseases (NIAID) provided funding to Miriam Braunstein under grant number AI054540.

REFERENCES

- Chatzi KE, Sardis MF, Economou A, Karamanou S. 2014. SecA-mediated targeting and translocation of secretory proteins. *Biochim Biophys Acta* 1843:1466–1474. <http://dx.doi.org/10.1016/j.bbamcr.2014.02.014>.
- Gouridis G, Karamanou S, Gelis I, Kalodimos CG, Economou A. 2009. Signal peptides are allosteric activators of the protein translocase. *Nature* 462:363–367. <http://dx.doi.org/10.1038/nature08559>.
- Feltcher ME, Braunstein M. 2012. Emerging themes in SecA2-mediated protein export. *Nat Rev Microbiol* 10:779–789. <http://dx.doi.org/10.1038/nrmicro2874>.
- Bensing BA, Seepersaud R, Yen YT, Sullam PM. 2014. Selective transport by SecA2: an expanding family of customized motor proteins. *Biochim Biophys Acta* 1843:1674–1686. <http://dx.doi.org/10.1016/j.bbamcr.2013.10.019>.
- Braunstein M, Brown AM, Kurtz S, Jacobs WR, Jr. 2001. Two nonredundant SecA homologues function in mycobacteria. *J Bacteriol* 183:6979–6990. <http://dx.doi.org/10.1128/JB.183.24.6979-6990.2001>.
- Sasseti CM, Rubin EJ. 2003. Genetic requirements for mycobacterial survival during infection. *Proc Natl Acad Sci U S A* 100:12989–12994. <http://dx.doi.org/10.1073/pnas.2134250100>.
- Braunstein M, Espinosa BJ, Chan J, Belisle JT, Jacobs WR, Jr. 2003. SecA2 functions in the secretion of superoxide dismutase A and in the virulence of *Mycobacterium tuberculosis*. *Mol Microbiol* 48:453–464. <http://dx.doi.org/10.1046/j.1365-2958.2003.03438.x>.
- Kurtz S, McKinnon KP, Runge MS, Ting JP, Braunstein M. 2006. The SecA2 secretion factor of *Mycobacterium tuberculosis* promotes growth in macrophages and inhibits the host immune response. *Infect Immun* 74:6855–6864. <http://dx.doi.org/10.1128/IAI.01022-06>.
- Sullivan JT, Young EF, McCann JR, Braunstein M. 2012. The *Mycobacterium tuberculosis* SecA2 system subverts phagosome maturation to promote growth in macrophages. *Infect Immun* 80:996–1006. <http://dx.doi.org/10.1128/IAI.05987-11>.
- van der Woude AD, Stoop EJ, Stiess M, Wang S, Ummels R, van Stempvoort G, Piersma SR, Cascioferro A, Jimenez CR, Houben EN, Luijckx J, Pieters J, van der Sar AM, Bitter W. 2014. Analysis of SecA2-dependent substrates in *Mycobacterium marinum* identifies protein kinase G (PknG) as a virulence effector. *Cell Microbiol* 16:280–295. <http://dx.doi.org/10.1111/cmi.12221>.
- Break TJ, Jun S, Indramohan M, Carr KD, Sieve AN, Dory L, Berg RE. 2012. Extracellular superoxide dismutase inhibits innate immune responses and clearance of an intracellular bacterial infection. *J Immunol* 188:3342–3350. <http://dx.doi.org/10.4049/jimmunol.1102341>.
- Hinchey J, Lee S, Jeon BY, Basaraba RJ, Venkataswamy MM, Chen B, Chan J, Braunstein M, Orme IM, Derrick SC, Morris SL, Jacobs WR, Jr, Porcelli SA. 2007. Enhanced priming of adaptive immunity by a proapoptotic mutant of *Mycobacterium tuberculosis*. *J Clin Invest* 117:2279–2288. <http://dx.doi.org/10.1172/JCI131947>.
- Lenz LL, Mohammadi S, Geissler A, Portnoy DA. 2003. SecA2-dependent secretion of autolytic enzymes promotes *Listeria monocytogenes* pathogenesis. *Proc Natl Acad Sci U S A* 100:12432–12437. <http://dx.doi.org/10.1073/pnas.2133653100>.
- Siboo IR, Chambers HF, Sullam PM. 2005. Role of SraP, a serine-rich surface protein of *Staphylococcus aureus*, in binding to human platelets. *Infect Immun* 73:2273–2280. <http://dx.doi.org/10.1128/IAI.73.4.2273-2280.2005>.
- Wu H, Mintz KP, Ladha M, Fives-Taylor PM. 1998. Isolation and characterization of FapI, a fimbriae-associated adhesin of *Streptococcus parasanguis* FW213. *Mol Microbiol* 28:487–500. <http://dx.doi.org/10.1046/j.1365-2958.1998.00805.x>.
- Xiong YQ, Bensing BA, Bayer AS, Chambers HF, Sullam PM. 2008. Role of the serine-rich surface glycoprotein GspB of *Streptococcus gordonii* in the pathogenesis of infective endocarditis. *Microb Pathog* 45:297–301. <http://dx.doi.org/10.1016/j.micpath.2008.06.004>.
- Nguyen-Mau SM, Oh SY, Kern VJ, Missiakas DM, Schneewind O. 2012. Secretion genes as determinants of *Bacillus anthracis* chain length. *J Bacteriol* 194:3841–3850. <http://dx.doi.org/10.1128/JB.00384-12>.
- Fagan RP, Fairweather NF. 2011. *Clostridium difficile* has two parallel and essential Sec secretion systems. *J Biol Chem* 286:27483–27493. <http://dx.doi.org/10.1074/jbc.M111.263889>.
- Takamatsu D, Bensing BA, Sullam PM. 2004. Four proteins encoded in the gspB-secY2A2 operon of *Streptococcus gordonii* mediate the intracellular glycosylation of the platelet-binding protein GspB. *J Bacteriol* 186:7100–7111. <http://dx.doi.org/10.1128/JB.186.21.7100-7111.2004>.
- Caspers M, Freudl R. 2008. *Corynebacterium glutamicum* possesses two secA homologous genes that are essential for viability. *Arch Microbiol* 189:605–610. <http://dx.doi.org/10.1007/s00203-008-0351-0>.
- Feltcher ME, Gunawardena HP, Zulauf KE, Malik S, Griffin JE, Sasseti CM, Chen X, Braunstein M. 2015. Label-free quantitative proteomics reveals a role for the *Mycobacterium tuberculosis* SecA2 pathway in exporting solute binding proteins and Mce transporters to the cell wall. *Mol Cell Proteomics* 14:1501–1516. <http://dx.doi.org/10.1074/mcp.M114.044685>.
- Gibbons HS, Wolschendorf F, Abshire M, Niederweis M, Braunstein M. 2007. Identification of two *Mycobacterium smegmatis* lipoproteins exported by a SecA2-dependent pathway. *J Bacteriol* 189:5090–5100. <http://dx.doi.org/10.1128/JB.00163-07>.
- Feltcher ME, Gibbons HS, Ligon LS, Braunstein M. 2013. Protein export by the mycobacterial SecA2 system is determined by the pre-protein mature domain. *J Bacteriol* 195:672–681. <http://dx.doi.org/10.1128/JB.02032-12>.
- DeLisa MP, Tullman D, Georgiou G. 2003. Folding quality control in the export of proteins by the bacterial twin-arginine translocation pathway. *Proc Natl Acad Sci U S A* 100:6115–6120. <http://dx.doi.org/10.1073/pnas.0937838100>.
- Nouwen N, Berrelkamp G, Driessen AJ. 2007. Bacterial Sec-translocase unfolds and translocates a class of folded protein domains. *J Mol Biol* 372:422–433. <http://dx.doi.org/10.1016/j.jmb.2007.07.003>.
- Weiss JB, Ray PH, Bassford PJ, Jr. 1988. Purified SecB protein of *Escherichia coli* retards folding and promotes membrane translocation of the maltose-binding protein in vitro. *Proc Natl Acad Sci U S A* 85:8978–8982. <http://dx.doi.org/10.1073/pnas.85.23.8978>.
- Kusters I, Driessen AJ. 2011. SecA, a remarkable nanomachine. *Cell Mol Life Sci* 68:2053–2066. <http://dx.doi.org/10.1007/s00018-011-0681-y>.
- Hou JM, D’Lima NG, Rigel NW, Gibbons HS, McCann JR, Braunstein M, Teschke CM. 2008. ATPase activity of *Mycobacterium tuberculosis* SecA1 and SecA2 proteins and its importance for SecA2 function in macrophages. *J Bacteriol* 190:4880–4887. <http://dx.doi.org/10.1128/JB.00412-08>.
- Rigel NW, Gibbons HS, McCann JR, McDonough JA, Kurtz S, Braunstein M. 2009. The accessory SecA2 system of mycobacteria requires ATP binding and the canonical SecA1. *J Biol Chem* 284:9927–9936. <http://dx.doi.org/10.1074/jbc.M900325200>.
- Ligon LS, Rigel NW, Romanchuk A, Jones CD, Braunstein M. 2013. Suppressor analysis reveals a role for SecY in the SecA2-dependent protein export pathway of mycobacteria. *J Bacteriol* 195:4456–4465. <http://dx.doi.org/10.1128/JB.00630-13>.
- Sharma V, Arockiasamy A, Ronning DR, Savva CG, Holzenburg A, Braunstein M, Jacobs WR, Jr, Sacchettini JC. 2003. Crystal structure of *Mycobacterium tuberculosis* SecA, a preprotein translocating ATPase. *Proc Natl Acad Sci U S A* 100:2243–2248. <http://dx.doi.org/10.1073/pnas.0538077100>.
- Papanikolaou Y, Papadovasilaki M, Ravelli RB, McCarthy AA, Cusack S, Economou A, Petratos K. 2007. Structure of dimeric SecA, the *Escherichia coli* preprotein translocase motor. *J Mol Biol* 366:1545–1557. <http://dx.doi.org/10.1016/j.jmb.2006.12.049>.
- Hunt JF, Weinkauff S, Henry L, Fak JJ, McNicholas P, Oliver DB, Deisenhofer J. 2002. Nucleotide control of interdomain interactions in the conformational reaction cycle of SecA. *Science* 297:2018–2026. <http://dx.doi.org/10.1126/science.1074424>.
- Zimmer J, Nam Y, Rapoport TA. 2008. Structure of a complex of the ATPase SecA and the protein-translocation channel. *Nature* 455:936–943. <http://dx.doi.org/10.1038/nature07335>.
- Vassilyev DG, Mori H, Vassilyeva MN, Tsukazaki T, Kimura Y, Tahirov TH, Ito K. 2006. Crystal structure of the translocation ATPase SecA from *Thermus thermophilus* reveals a parallel, head-to-head dimer. *J Mol Biol* 364:248–258. <http://dx.doi.org/10.1016/j.jmb.2006.09.061>.
- Erlanson KJ, Miller SB, Nam Y, Osborne AR, Zimmer J, Rapoport TA.

2008. A role for the two-helix finger of the SecA ATPase in protein translocation. *Nature* 455:984–987. <http://dx.doi.org/10.1038/nature07439>.
37. Whitehouse S, Gold VA, Robson A, Allen WJ, Sessions RB, Collinson I. 2012. Mobility of the SecA 2-helix-finger is not essential for polypeptide translocation via the SecYEG complex. *J Cell Biol* 199:919–929. <http://dx.doi.org/10.1083/jcb.201205191>.
 38. Chen Y, Bauer BW, Rapoport TA, Gumbart JC. 2015. Conformational changes of the clamp of the protein translocation ATPase SecA. *J Mol Biol* 427:2348–2359. <http://dx.doi.org/10.1016/j.jmb.2015.05.003>.
 39. Osborne AR, Clemons WM, Jr, Rapoport TA. 2004. A large conformational change of the translocation ATPase SecA. *Proc Natl Acad Sci U S A* 101:10937–10942. <http://dx.doi.org/10.1073/pnas.0401742101>.
 40. Gelis I, Bonvin AM, Keramisanou D, Koukaki M, Gouridis G, Karamanou S, Economou A, Kalodimos CG. 2007. Structural basis for signal-sequence recognition by the translocase motor SecA as determined by NMR. *Cell* 131:756–769. <http://dx.doi.org/10.1016/j.cell.2007.09.039>.
 41. Bauer BW, Rapoport TA. 2009. Mapping polypeptide interactions of the SecA ATPase during translocation. *Proc Natl Acad Sci U S A* 106:20800–20805. <http://dx.doi.org/10.1073/pnas.0910550106>.
 42. Bhanu MK, Zhao P, Kendall DA. 2013. Mapping of the SecA signal peptide binding site and dimeric interface by using the substituted cysteine accessibility method. *J Bacteriol* 195:4709–4715. <http://dx.doi.org/10.1128/JB.00661-13>.
 43. DeJesus MA, Sacchetti JC, Ioerger TR. 2013. Reannotation of translational start sites in the genome of *Mycobacterium tuberculosis*. *Tuberculosis (Edinb)* 93:18–25. <http://dx.doi.org/10.1016/j.tube.2012.11.012>.
 44. Studier FW. 2005. Protein production by auto-induction in high density shaking cultures. *Protein Expr Purif* 41:207–234. <http://dx.doi.org/10.1016/j.pep.2005.01.016>.
 45. Heras B, Martin JL. 2005. Post-crystallization treatments for improving diffraction quality of protein crystals. *Acta Crystallogr D Biol Crystallogr* 61:1173–1180. <http://dx.doi.org/10.1107/S0907444905019451>.
 46. Leahy DJ, Hendrickson WA, Aukhil I, Erickson HP. 1992. Structure of a fibronectin type III domain from tenascin phased by MAD analysis of the selenomethionyl protein. *Science* 258:987–991. <http://dx.doi.org/10.1126/science.1279805>.
 47. Fischetti RF, Xu S, Yoder DW, Becker M, Nagarajan V, Sanishvili R, Hilgart MC, Stepanov S, Makarov O, Smith JL. 2009. Mini-beam collimator enables microcrystallography experiments on standard beamlines. *J Synchrotron Radiat* 16:217–225. <http://dx.doi.org/10.1107/S0909049508040612>.
 48. Otwinowski Z, Minor W. 1997. Processing of X-ray diffraction data collected in oscillation mode. *Macromol Crystallogr A* 276:307–326. [http://dx.doi.org/10.1016/S0076-6879\(97\)76066-X](http://dx.doi.org/10.1016/S0076-6879(97)76066-X).
 49. Sheldrick GM. 2010. Experimental phasing with SHELXC/D/E: combining chain tracing with density modification. *Acta Crystallogr D Biol Crystallogr* 66:479–485. <http://dx.doi.org/10.1107/S0907444909038360>.
 50. Vonnrhein C, Blanc E, Roversi P, Bricogne G. 2007. Automated structure solution with autoSHARP. *Methods Mol Biol* 364:215–230.
 51. Emsley P, Lohkamp B, Scott WG, Cowtan K. 2010. Features and development of Coot. *Acta Crystallogr D Biol Crystallogr* 66:486–501. <http://dx.doi.org/10.1107/S0907444910007493>.
 52. Read RJ. 1986. Improved Fourier coefficients for maps using phases from partial structures with errors. *Acta Crystallogr A* 42:140–149. <http://dx.doi.org/10.1107/S0108767386099622>.
 53. Cowtan KD, Main P. 1996. Phase combination and cross validation in iterated density-modification calculations. *Acta Crystallogr D Biol Crystallogr* 52:43–48. <http://dx.doi.org/10.1107/S090744499500761X>.
 54. Hunt JF, Deisenhofer J. 2003. Ping-pong cross-validation in real space: a method for increasing the phasing power of a partial model without risk of model bias. *Acta Crystallogr D Biol Crystallogr* 59:214–224. <http://dx.doi.org/10.1107/S0907444902018930>.
 55. Bricogne GBE, Brandl M, Flensburg C, Keller P, Paciorek W, Roversi PSA, Smart OS, Vonnrhein C, Womack TO. 2011. BUSTER version 2.8.0. Global Phasing Ltd., Cambridge, United Kingdom.
 56. Guo XV, Monteleone M, Klotzsche M, Kamionka A, Hillen W, Braustein M, Ehrt S, Schnappinger D. 2007. Silencing *Mycobacterium smegmatis* by using tetracycline repressors. *J Bacteriol* 189:4614–4623. <http://dx.doi.org/10.1128/JB.00216-07>.
 57. Dauter Z, Dauter M, Dodson E. 2002. Jolly SAD. *Acta Crystallogr D Biol Crystallogr* 58:494–506. <http://dx.doi.org/10.1107/S090744490200118X>.
 58. Das S, Grady LM, Michtav J, Zhou Y, Cohan FM, Hingorani MM, Oliver DB. 2012. The variable subdomain of *Escherichia coli* SecA functions to regulate SecA ATPase activity and ADP release. *J Bacteriol* 194:2205–2213. <http://dx.doi.org/10.1128/JB.00039-12>.
 59. Gold VA, Whitehouse S, Robson A, Collinson I. 2013. The dynamic action of SecA during the initiation of protein translocation. *Biochem J* 449:695–705. <http://dx.doi.org/10.1042/BJ20121314>.
 60. Das S, Oliver DB. 2011. Mapping of the SecA-SecY and SecA-SecE interfaces by site-directed *in vivo* photocross-linking. *J Biol Chem* 286:12371–12380. <http://dx.doi.org/10.1074/jbc.M110.182931>.
 61. Zimmer J, Rapoport TA. 2009. Conformational flexibility and peptide interaction of the translocation ATPase SecA. *J Mol Biol* 394:606–612. <http://dx.doi.org/10.1016/j.jmb.2009.10.024>.
 62. Vrontou E, Karamanou S, Baud C, Sianidis G, Economou A. 2004. Global co-ordination of protein translocation by the SecA IRA1 switch. *J Biol Chem* 279:22490–22497. <http://dx.doi.org/10.1074/jbc.M401008200>.
 63. Duong F, Wickner W. 1999. The PrlA and PrlG phenotypes are caused by a loosened association among the translocase SecYEG subunits. *EMBO J* 18:3263–3270. <http://dx.doi.org/10.1093/emboj/18.12.3263>.
 64. Oliver DB, Beckwith J. 1982. Regulation of a membrane component required for protein secretion in *Escherichia coli*. *Cell* 30:311–319. [http://dx.doi.org/10.1016/0092-8674\(82\)90037-X](http://dx.doi.org/10.1016/0092-8674(82)90037-X).
 65. Ding H, Hunt JF, Mukerji I, Oliver D. 2003. *Bacillus subtilis* SecA ATPase exists as an antiparallel dimer in solution. *Biochemistry* 42:8729–8738. <http://dx.doi.org/10.1021/bi0342057>.
 66. Auclair SM, Oliver DB, Mukerji I. 2013. Defining the solution state dimer structure of *Escherichia coli* SecA using Forster resonance energy transfer. *Biochemistry* 52:2388–2401. <http://dx.doi.org/10.1021/bi301217t>.
 67. D’Lima NG, Teschke CM. 2013. ADP-dependent conformational changes distinguish *Mycobacterium tuberculosis* SecA2 from SecA1. *J Biol Chem* 289:2307–2317. <http://dx.doi.org/10.1074/jbc.M113.533323>.
 68. Zhou J, Xu Z. 2003. Structural determinants of SecB recognition by SecA in bacterial protein translocation. *Nat Struct Biol* 10:942–947. <http://dx.doi.org/10.1038/nsb980>.
 69. Schneewind O, Missiakas DM. 2012. Protein secretion and surface display in Gram-positive bacteria. *Philos Trans R Soc Lond B Biol Sci* 367:1123–1139. <http://dx.doi.org/10.1098/rstb.2011.0210>.
 70. de Keyser J, van der Sluis EO, Spelbrink RE, Nijstad N, de Kruijff B, Nouwen N, van der Does C, Driessen AJ. 2005. Covalently dimerized SecA is functional in protein translocation. *J Biol Chem* 280:35255–35260. <http://dx.doi.org/10.1074/jbc.M506157200>.
 71. Jilaveanu LB, Zito CR, Oliver D. 2005. Dimeric SecA is essential for protein translocation. *Proc Natl Acad Sci U S A* 102:7511–7516. <http://dx.doi.org/10.1073/pnas.0502774102>.
 72. Gouridis G, Karamanou S, Sardis MF, Scharer MA, Capitani G, Economou A. 2013. Quaternary dynamics of the SecA motor drive translocase catalysis. *Mol Cell* 52:655–666. <http://dx.doi.org/10.1016/j.molcel.2013.10.036>.
 73. Prabudiansyah I, Kusters I, Driessen AJ. 2015. *In vitro* interaction of the housekeeping SecA1 with the accessory SecA2 protein of *Mycobacterium tuberculosis*. *PLoS One* 10:e0128788. <http://dx.doi.org/10.1371/journal.pone.0128788>.
 74. Durack J, Burke TP, Portnoy DA. 2015. A *prl* mutation in SecY suppresses secretion and virulence defects of *Listeria monocytogenes secA2* mutants. *J Bacteriol* 197:932–42. <http://dx.doi.org/10.1128/JB.02284-14>.